Neuro-Oncology 14(8):1037–1049, 2012.
doi:10.1093/neuonc/nos121
Advance Access publication June 14, 2012

CD38 deficiency in the tumor microenvironment attenuates glioma progression and modulates features of tumor-associated microglia/macrophages

Ayelet Levy, Eran Blacher, Hananya Vaknine, Frances E. Lund, Reuven Stein, and Lior Mayo

Department of Neurobiology, George S. Wise Faculty of Life Sciences, Tel Aviv University, Ramat Aviv, Israel (A.L., E.B., R.S., L.M.); Institute of Pathology, E. Wolfson Medical Center, Holon, Israel (H.V.); Department of Medicine, Division of Allergy, Immunology and Rheumatology, University of Rochester, Rochester, New York (F.E.L.); Center for Neurologic Diseases, Brigham and Women's Hospital, Harvard Medical School, Boston, Massachusetts (L.M.)

Gliomas are the most frequent primary tumors of the brain, and for highly malignant gliomas there is no successful treatment. The tumor microenvironment contains large numbers of infiltrating microglia and macrophages (MM). There is increasing evidence that the tumor-associated MM support glioma expansion. CD38 is a multifunctional ectoenzyme that uses nicotinamide adenine dinucleotide as a substrate to generate second messengers. Previously we showed that CD38 deficiency modulates microglial "activation" and impaired recovery from head trauma by a microglia-associated mechanism. In view of the supportive role of MM in glioma progression and the role of CD38 in microglia activation, we hypothesize that deficiency of CD38 in the tumor microenvironment would inhibit glioma progression. Using the syngeneic GL261 model of glioma progression in wild-type and CD38 null mice, we show here that CD38 deficiency significantly attenuates glioma expansion and prolongs the life span of the glioma-bearing mice. The CD38 deficiency effect was associated with increased cell death and decreased metalloproteinase-12 expression in the tumor mass, as well as modulation of the tumor-induced MM properties, as indicated by a reduction in the expression of the MM marker F4/80 and matrix metalloproteinases. Our results thus suggest that CD38 participates in the tumor-supporting action of MM and that targeting CD38 might be a potential therapeutic approach for glioma treatment.

Keywords: brain, cancer, CD38, glioma, microglia.

Gliomas are the most common primary tumors of the brain. Despite aggressive treatment, the prognosis of highly malignant gliomas is poor. Increasing evidence suggests that glioma progression is regulated by the tumor microenvironment. Microglia/macrophages (MM) are the major microenvironmental cells in the tumor, constituting up to 40% of the tumor mass.[1]

Microglia are the resident immune, myeloid-originated cells of the CNS. In a healthy CNS, microglia survey the brain's environment for damage or perturbation of homeostasis. Once they sense such a condition, they respond by acquiring various features, collectively termed *activation*. Activated microglia have been suggested to play both beneficial and harmful roles in various brain pathologies, including neurodegenerative diseases and acute injuries.[2] In pathological conditions, macrophages infiltrate the brain and act together with the resident microglia. Since it is difficult to distinguish between microglia and macrophages, we refer to these cells in pathological conditions as MM.

Although the tumor-associated (T)MM may act as tumor suppressors by secreting free radicals and by recruiting cells of the adaptive immune system, compelling evidence demonstrates that they promote glioma progression and metastasis (for review, see Badie and

Received June 9, 2011; accepted April 18, 2012.

Corresponding Author: R. Stein, Department of Neurobiology, George S. Wise Faculty of Life Sciences, Tel Aviv University, Ramat Aviv, Tel Aviv, Israel 69978 (reuvens@post.tau.ac.il).

Schartner,[1] Watters, Schartner, and Badie,[3] and Yang et al.[4]). TMM are attracted toward glioma in large numbers, and the TMM density in gliomas positively correlates with tumor grade. TMM can release many factors, including extracellular matrix proteases and cytokines, which may directly or indirectly influence tumor invasiveness and proliferation.[1] Furthermore, depletion of microglia from organotypic brain slices[5] or TMM from the tumor area in vivo[6] largely impedes glioma expansion. Thus, abrogating the tumor-supporting effect of TMM may provide a new therapeutic approach to treat glioma. This may be achieved by targeting molecules known to modulate microglia responses to activation signals. Previously, we[7,8] and others[9] demonstrated that CD38 regulates microglial activation. A role of CD38 in microglial function was also shown in vivo in a head trauma model where CD38 deficiency reduced the accumulation of activated MM in the injured brain area and worsened the recovery of the mice from the trauma.[10] CD38 is a nicotinamide adenine dinucleotide (NAD) glycohydrolase and ADP-ribosyl cyclase. It is expressed by various cell types, including myeloid-derived cells. The extracellular enzymatic domain of CD38 uses NAD+ and NADP+ to catalyze the formation of the calcium-mobilizing metabolites adenosine diphosphate ribose (ADPR), cyclic ADPR, and nicotinic acid adenine dinucleotide phosphate. Notably, CD38 may also act as a cell-surface receptor.[11] CD38 can play a role in several biological systems, as indicated by studies using CD38-deficient mice. Accordingly, CD38 deficiency may impair both innate and adaptive immune responses. These include impaired neutrophile, monocyte, and dendritic cell trafficking and impaired T cell priming, as well as reduced humoral responses and enhanced susceptibility to infection.[12,13] Additional effects associated with CD38 deficiency include attenuation of airway hyperreactivity[14] and impairments of insulin secretion,[15] osteoclast-mediated bone resorption,[16] and oxytocin secretion.[17] In cells of the immune system, levels of CD38 expression may vary as functions of the activation state, in a manner that is cell-type dependent. In T cells and in cells of the myeloid lineage, for example, the levels of expression increase upon activation.[18]

The expression of CD38 is also relevant in neoplastic cells. Specifically, in chronic lymphocytic leukemia, a high percentage of CD38-expressing leukemic cells is associated with unfavorable prognosis, as well as with cell activation and proliferation.[19]

In view of our previous results that CD38 regulates microglial activation, we reasoned that targeting CD38 in the tumor microenvironment may attenuate glioma progression. To test this hypothesis, glioma expansion was examined in wild-type (WT) or $Cd38^{-/-}$ C57BL/6 mice intracranially injected with the syngeneic glioma GL261 cells. Our results show that CD38 deficiency delayed glioma progression, ie reduced tumor volume and moderately prolonged survival duration of tumor-bearing mice. The reduction in the tumor volume was associated with enhanced cell death in the tumor mass as well as modulation of TMM features.

Materials and Methods

Reagents

Reagents used were purchased from Sigma, unless indicated otherwise.

Antibodies

The following primary antibodies were used: rabbit anti-ionized calcium-binding adaptor molecule 1 (Iba1) polyclonal antibody (Ab; 019-19741, Wako Chemicals); rat anti-mouse F4/80 monoclonal (m)Ab (MCA497, Serotec); rabbit anti-glial fibrillary acidic protein (GFAP) polyclonal Abs (Z 0334, Dako Cytomation); rat anti-CD31 mAb (550274, BD Pharmingen); rabbit anti–matrix metalloproteinase (MMP)–12 mAb (ab52897, Abcam); mouse anti-β tubulin (T4026, Sigma); rabbit anti-glyceraldehyde 3-phosphate dehydrogenase (GAPDH) (2118, Cell Signaling Technology); and rat anti-5-bromo-2′-deoxyuridine (BrdU) mAb (ab6326, Abcam). The secondary Abs used for 3,3′-diaminobenzidine (DAB) chromogenic staining were as follows: biotin-conjugated rabbit anti-rat (BA-4001, Vector Laboratories) (for F4/80, BrdU, and CD31 staining) diluted 1:200 and biotin-conjugated goat anti-rabbit (BA-1000, Vector Laboratories) (for Iba1, GFAP, and MMP-12 staining) diluted 1:200.

The following Abs were used for flow cytometric analyses: phycoerythrin (PE)-conjugated rat anti-CD38 (NIMR-5, 1635-09, Southern Biotech); Alexa Fluor 488–conjugated rat anti-CD11b (M1/70, 101219); allophycocyanin (APC)-conjugated rat anti-CD45 (30-F11, 103111); APC-conjugated Armenian hamster anti-CD3ε (145-2C11, 100311); PE-conjugated rat anti-CD8a (53-6.7, 100707); fluorescein isothiocynate (FITC)–conjugated rat anti-CD4 (GK1.5, 100405); PE-conjugated rat anti-CD11b (M1/70, 101207); APC-conjugated rat immunoglobulin (Ig)G2b (RTK4530, 400611); PE-conjugated rat IgG2b (RTK4530, 400607); FITC-conjugated rat IgG2b (RTK4530, 400605); and APC-conjugated Armenian hamster IgG (HTK888, 400911, BioLegend).

Mice

C57BL/6J CD38-deficient mice ($Cd38^{-/-}$)[20,21] were obtained from the Trudeau Institute Breeding Facility. The animals used in the present experiments were backcrossed for 12 generations to C57BL/6J.[13] WT ($Cd38^{+/+}$) C57BL/6J (catalog number 2BL/610) mice were purchased from Harlan. Mice were maintained and treated in accordance with all applicable rules and guidelines of the Animal Care and Use Committee of Tel Aviv University.

Cell Culture

The GL261 glioma cells were provided by Professor Geza Safrany (Department of Molecular and Tumor

Radiobiology, Budapest, Hungary) and were maintained in Dulbecco's modified Eagle's medium (DMEM; Gibco BRL), supplemented with 10% fetal calf serum (FCS), 1% penicillin-streptomycin, and 4 mM L-glutamine and grown at 37°C with 5% CO_2. Green fluorescent protein (GFP)–expressing GL261 (GFP-GL261) was generated by infection of GL261 cells with the pHR′ cytomegalovirus GFP virus.[22] GFP-expressing cells were isolated by a FACSAria fluorescence-activated cell sorter (Becton Dickinson).

Intracranial Injection of GL261 Glioma Cells and MRI

Four-month-old male WT and $Cd38^{-/-}$ C57BL/6 mice were anesthetized by an i.p. injection of ketamine (100 mg/kg) and xylazine (20 mg/kg) and placed in a Kopf Stereotaxic Alignment System. An approximately 1-cm-long cut was made in the scalp, and the skull was exposed. Then, a 2-mm burr hole was drilled 1 mm posterior to the bregma and 1.5 mm lateral to it. Using a Hamilton 10-μL syringe and a 31-g Hamilton needle, we injected 5×10^3 or 1×10^5 GL261 or GFP-GL261 cells in 3 μL DMEM 3 mm below the cortical surface, at a rate of 1 μL/min. In order to avoid backflow, the needle was left for an additional 1 min before being gradually removed. The scalp was stitched and the mice were allowed to recover in their cages.

Magnetic Resonance Imaging

Following injection, at days 17 and 21 (when 5×10^3 GL261 cells were injected) or at days 10, 14, and 17 (when 1×10^5 GL261 cells were injected), tumor progression was assessed by gadolinium (Gd)-diethylenetriamine pentacetate (DTPA)–enhanced T1-weighted MRI (Bruker, Biospin). The MRI scans were performed under inhalational 1%–2% isoflurane (Nicholas Piramal) anesthesia in 98% oxygen. Immediately before scan, mice were i.p. injected with 150 μL of 0.1-M Gd-DTPA (Soreq Radiopharmaceuticals). Mice were scanned in a 7T/30 spectrometer (Bruker, Biospin) using a quadrature head coil and a 400-mT/m gradient system. The MRI protocol included Gd-DTPA–enhanced T1-weighted MRI (repetition time = 800 ms and echo time = 12 ms). The field of view was 2 × 2 cm with matrix dimensions of 256 × 128 pixels (reconstructed to 256 × 256). Fourteen slices 0.8 mm thick and with no gap were acquired in coronal orientation. The final image resolution was $0.078 \times 0.078 \times 1$ mm^3. The tumor area was determined using Medical Image Analysis v.2.4 in MatLab.

Survival Analysis

Following injection of the GL261 cells, mice were monitored and weighed daily. The endpoint was defined by a lack of physical activity and more than 15% reduction in body weight. The probability of survival was calculated using the Kaplan–Meier method, and statistical analysis was performed using a log-rank test.

BrdU Injection

Twenty days after injection of GFP-GL261 cells, BrdU was i.p. injected into the mice (50 mg/kg). Two hours later, the mice were killed and their brains were processed for immunostaining.

Immunoblot Analysis

Twenty-nine days following injection of GL261 cells, mice that reached the death criteria for survival analysis were overdosed with ketamine/xylazine and subsequently perfused. Brains were removed, and the tumor-bearing hemisphere was homogenized and lysed for protein extraction. Alternatively protein extracts were prepared from isolated TMM. Thirty to one hundred micrograms of protein from the different samples were separated by 10% or 12.5% sodium dodecyl sulfate polyacrylamide gel electrophoresis and electroblotted onto supported nitrocellulose. Each blot was blocked for 1 h in Tris-buffered saline/Tween-20 (10 mM Tris base, 150 mM NaCl, 0.05% Tween-20) containing 5% fat-free milk and then incubated overnight at 4°C with a primary Ab (anti–MMP-12, 1:1000; anti-tubulin, 1:2500; anti-GAPDH, 1:1000). After washing the membranes 3 times (10 min each) with Tris-buffered saline/Tween-20, we incubated the samples for 1 h at room temperature with the appropriate second Ab (goat anti-mouse or goat anti-rabbit IgG peroxidase conjugate, Jackson ImmunoResearch Laboratories). Blots were developed using the Supersignal West Pico Chemiluminescent Substrate kit (Pierce Biotechnology). Each blot was reprobed with anti-tubulin mAb or anti-GAPDH to verify that proteins were uniformly loaded across the gel. The signal, normalized to tubulin or GAPDH, was quantified by the use of EZQuant-Gel software.

Immunostaining

Twenty days following injection of GL261 cells, mice were overdosed with ketamine/xylazine and subsequently perfused and fixed as described.[10] Frozen coronal sections (30 μm) were then cut on a sliding microtome. For pathological analysis of the mitotic cells and for terminal deoxynucleotidyl transferase (2'-deoxyuridine 5'-triphosphate) nick end labeling TUNEL staining, brains were embedded in paraffin and cut into 6-μm sections.

The free-floating sections[23] were immunostained as described previously,[10] utilizing the following primary Abs: Iba1 (1:1000), anti-F4/80 (1:100), anti-CD31 (1:100), anti-BrdU (1:200), and GFAP (1:2000). Staining was visualized with the aid of the appropriate biotinylated secondary Abs and horseradish peroxidase–conjugated streptavidin (Vectastain Elite ABC Kit [Standard], Vector Laboratories). For BrdU staining, sections were first incubated in 2 N HCl for 30 min at 37°C and neutralized by incubation in 0.1-M borate buffer. MMP-12 staining was performed on

paraffin-embedded sections (anti–MMP-12 [1:100]). TUNEL staining was performed on paraffin-embedded sections using the ApopTag Peroxidase In Situ Apoptosis Detection Kit (Millipore). Sections were photographed and image analysis performed using Image-Pro Plus v.5.1 (Media Cybernetics).

Image Analysis

The peroxidase-immunostained sections were viewed and photographed with a Nikon Plan ×4/0.1NA, Nikon Plan ×10/0.25NA, or Nikon Plan ×40/0.65NA objective and a Nikon DS-5M camera. Two to four slices covering representative areas of the entire tumor were captured. The tumor area was captured frame by frame in a ×4 magnification (for BrdU, F4/80, and Iba1 staining) (1−4 images per slice) or ×10 magnification (for CD31, TUNEL, and MMP-12 staining). For GFAP staining, every fourth frame in the tumor boundaries was captured in a ×40 magnification. The density of immunohistochemical staining was determined with the aid of Image-Pro Plus v.5.1 (Media Cybernetics) by expressing the amount of staining as a percentage of the area analyzed.

For analysis of mitotic cells, hematoxylin and eosin–stained 6-μm paraffin sections were examined. Two to four slices covering representative areas of the entire tumor were captured. In each slice, the number of mitotic cells was counted in 3 fields.

Isolation of MM

MM from adult mice were isolated as previously described,[24,25] with minor modifications. Briefly, mice were deeply anesthetized and then subjected to perfusion through the left ventricle with 10 mL of ice-cold sterile saline. Brains were then removed and the injected (right) hemispheres were processed as following. Three hemispheres were pooled and mechanically and enzymatically digested in 10 mL of digestion buffer (0.05% [w/v] collagenase type III, 0.5% Dispase II, 40 μg/mL DNAse I, 0.1 μg/mL *N*-alpha-p-tosyl-L-lysine chloromethyl ketone, 20 mM 4-(2-hydroxyethyl)-1-piperazineethanesulfonic acid [HEPES] in Hanks' balanced salt solution (HBSS). Enzymes were inactivated by addition of 20 mL of Ca^{2+}/Mg^{2+}-free HBSS containing 2 mM EDTA and 20 mM HEPES. The digested brain pieces were triturated and passed through a 100-μM cell strainer. Cells were centrifuged and resuspended in HBSS containing 30% isotonic Percoll and 40 μg/mL DNAse I, passed through a 70-μm cell strainer, and centrifuged at 1000 × *g* at 4°C for 25 min, and debris was removed. For isolation of MM, the cells were transferred to a new tube containing 20 mL of Ca^{2+}/Mg^{2+}-free phosphate buffered saline (PBS), 0.5% endotoxin and protease-free bovine serum albumin (BSA), and 2 mM EDTA. The cells were then incubated with CD11b-coated anti-mouse microbeads and passed through a magnetic cell separation column (Miltenyi Biotec) according to the manufacturer's instructions. The isolated $CD11b^+$ cells (ie, MM) were then either lysed in TRIzol (Invitrogen Life Science) for RNA preparation for quantitative reverse transcription (qRT-)PCR according to the manufacturer's instructions or lysed for preparation of protein extracts. Each $CD11b^+$ cell preparation was analyzed for purity by flow cytometry. Approximately 90% of the cells isolated by this procedure were identified as MM ($CD11b^+$/CD45) by use of the PE-conjugated CD11b and FITC-conjugated CD45 Abs (data not shown).

Isolation of Brain Cells for Flow Cytometry

The brains were processed as described for isolation of MM. Following the Percoll gradient step, cells were centrifuged (700 × *g*, 10 min, 4°C), and the resulting cell pellet was incubated (30 min, 4°C) in flow cytometry buffer (PBS supplemented with 1% BSA and 0.05% sodium azide) containing the appropriate fluorescence-conjugated Abs or their isotype-matched controls. After incubation, the cells were washed with the flow cytometry buffer. Antigen expression on 1×10^4 live cells was determined using a Becton Dickinson FACSort and analyzed using CellQuest and FlowJo 5.7.2 software.

qRT-PCR Analysis

Following total RNA isolation from the isolated MM, cDNA was synthesized using 0.5 μg total MM RNA as a template and random decamer primers in a 20-μL reaction volume using the SuperScript First-Strand Synthesis System (Invitrogen) according to the manufacturer's instructions. The cDNA (10 ng) obtained was used as a template for qRT-PCR using the ABsolute Blue SYBR Green PCR mix (ABgene) and appropriate primers (Supplementary material, Table S1; primer concentrations were optimized for each primer set) by the ABI 7300 Real-Time PCR System (Applied Biosystems). The following 3-stage program was employed as instructed by the manufacturer: 2 min at 50°C, 15 min at 95°C, then 40 cycles of 15 s at 95°C and 1 min at 60°C. Melting-curve analysis was used to assess primer specificity and product quality by stepwise denaturation of the PCR product. Relative levels of the different transcripts were quantified using the $2^{-\Delta\Delta CT}$ method.[26,27]

For the analysis of MMP mRNA levels in the TMM, data were classified into 2 groups: one corresponding to TMM isolated from middle-phase/-size tumors (based on the time post-injection or the tumor volume in MRI) and the second corresponding to large-phase/-size tumors.

Statistical Analysis

Data are presented as the mean ± SEM. A 2-way analysis of variance (ANOVA) was used to compare tumor volume (repeated measures) and MMP mRNA expression in TMM. The survival duration of the mice was analyzed by Kaplan–Meier survival analysis followed by a

log-rank test. Other experiments were analyzed by an unpaired Student's *t* test; $P < .05$ was considered statistically significant. In the analysis of the MMP-12 staining density, 1 WT mouse was regarded as an outlier and was excluded from statistical analysis ($P < .05$, Dixon's *Q*-test). Extreme values were identified by the outlier test of Dixon and Massey.[28]

Results

CD38 Deficiency Reduces Glioma Expansion and Extends the Life Span of Glioma-Bearing Mice

To assess the role of CD38 in the tumor microenvironment on glioma progression, we employed the syngeneic model of implantation of GL261 glioma cells into brains of WT and CD38-deficient mice. This model was used because it represents tumor characteristics similar to human glioblastoma multiforme.[29,30] We injected 5×10^3 GL261 cells into the brains of WT and $Cd38^{-/-}$ mice, and tumor volume was assessed by Gd-DTPA–enhanced T1-weighted MRI analysis at 17 and 21 days post-injection. As shown in Fig. 1A and 1B, the tumor growth in the $Cd38^{-/-}$ mice was significantly attenuated, and at 21 days post-injection it was 62% ($P = .00001$) smaller than in WT mice. Assessment of the survival of the glioma-bearing mice (Fig. 1C) revealed that $Cd38^{-/-}$ glioma–bearing mice survived significantly longer than WT-glioma–bearing mice (median survival of $Cd38^{-/-}$ mice was 30.5 vs 27 days in WT, $P = .0003$). The effect of CD38 deficiency on glioma was also examined under more aggressive conditions (injection of 1×10^5 cells), in which the tumor expanded faster (due to higher amount of injected glioma cells). As shown in Fig. 1D–F, also under this condition, CD38 deficiency significantly attenuated tumor growth (38% [$P = .002$], 17 days post-injection) and prolonged survival (Fig. 1G) (median survival of $Cd38^{-/-}$ mice was 25 vs 23 days in WT, $P = .03$). Taken together, these results demonstrate that CD38 deficiency in the tumor microenvironment significantly delays glioma progression.

Characterization of the Glioma Microenvironment in WT and $Cd38^{-/-}$ Mice

In view of these results, we next characterized and compared the glioma microenvironment of WT and $Cd38^{-/-}$ mice in an attempt to identify the cells in the glioma microenvironment that might account for the CD38 effect on glioma progression. To this end we compared the presence and features of cells known to be present in the tumor microenvironment and/or its vicinity between WT and $Cd38^{-/-}$ mice.

First we tested whether the accumulation of astrocytes in the tumors was affected by host expression of CD38. Brain sections of glioma-bearing mice were stained with anti-GFAP Abs. As shown in Fig. 2A, the astrocytes were largely excluded from the tumor mass but were highly enriched in the tumor border in both *Cd38* genotypes. The potential contribution of astrocytes to the CD38 effect was assessed by determining the density of GFAP staining in the tumor border. Figure 2B shows that the density of astrocytes in the tumor border was similar in both *Cd38* genotypes. Together, these results suggest that reactive astrocytes are not involved in the effect of CD38 in the tumor microenvironment on glioma progression.

Next, we examined the role of T cells in the CD38 effect on glioma progression by assessing the levels of T cells as well as T-helper and cytotoxic T cell subpopulations in the tumor vicinity. To this end the percentage of T cells (CD3-positive cells) of the immune cell population ($CD45^+$ cells) as well as the percentage of T-helper ($CD3^+/CD4^+$-positive cells) and cytotoxic T cells ($CD3^+/CD8^+$-positive cells) of the T cell population (CD3-positive cells) were determined in the tumor-bearing hemisphere by flow cytometry. The analysis revealed that the percentage of T cells of the total immune cell population was similar in both *Cd38* genotypes (Fig. 3A). Similarly, no significant difference was observed in the percentage of $CD4^+$ T cells (Fig. 3B). However, the percentage of $CD8^+$ T cells was lower in the $Cd38^{-/-}$ mice compared with WT mice. The similar accumulation of astrocytes and T cells and the reduction in the percentage of cytotoxic T cells imply that the CD38 deficiency effect is not mediated, at least directly, by these cells.

To assess the role of TMM in the CD38 effect on glioma progression, brain sections obtained from glioma-bearing mice were stained with anti-Iba1 (a marker for MM) Abs. Figure 4A shows that the tumor mass was massively populated by Iba1-positive cells, in particular in its borders. In addition, Iba1 staining was observed, although to a lesser extent, all over the brain. Staining with F4/80 Ab also revealed a massive accumulation of MM in the tumor; however, in contrast to Iba1, the F4/80-positive subpopulation was almost exclusively confined to the tumor mass (Fig. 4B). Assessment of the amount of MM (Iba1-positive cells) in the tumor area revealed that the density of Iba1-positive cells in the tumor area was similar in both *Cd38* genotypes (Fig. 4C). Similarly, no significant difference was observed when the percentage of CD11b-positive cells (marker for MM) of the total immune cell population (CD45-positive cells) in the tumor-bearing hemisphere was determined by flow cytometry (Fig. 4D). However, examination of the density of F4/80-positive cells revealed that it was significantly lower (30%) in the tumor area in $Cd38^{-/-}$ mice compared with WT mice (Fig. 4E). These results suggest that CD38 deficiency does not affect the amount of MM in the tumor mass but rather may alter their properties. Furthermore, the results also suggest that the CD38-deficiency–mediated changes in the TMM properties may play a role in the inhibition of glioma progression in $Cd38^{-/-}$ mice. To further explore whether CD38 can directly affect the TMM, we examined whether these cells express CD38 and the effect of the tumor on such expression. CD38 expression was determined by flow cytometry in CD11b-positive cells

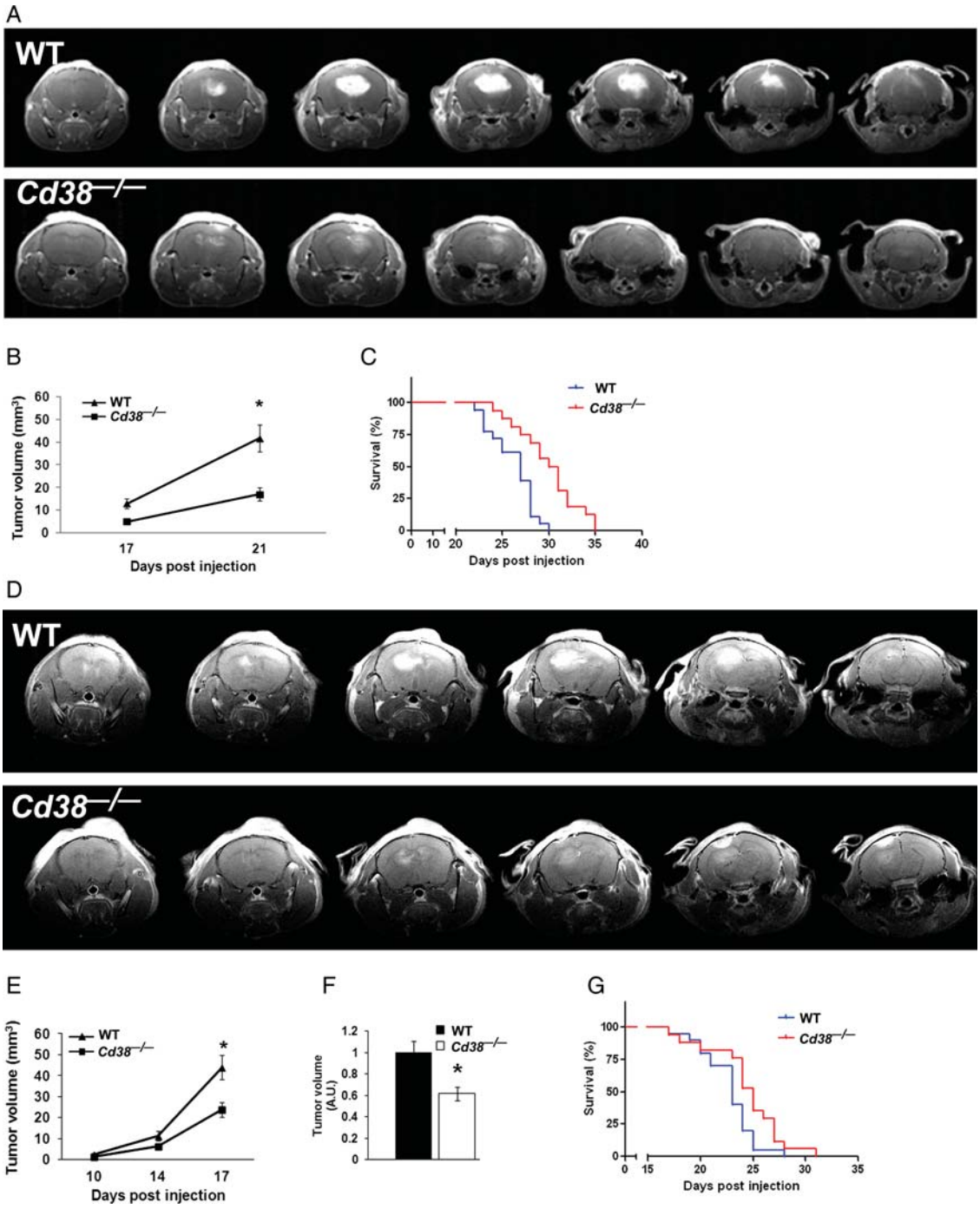

Fig. 1. CD38 deficiency reduces tumor volume and prolongs survival duration of glioma-bearing mice. WT and $Cd38^{-/-}$ male mice were i.c. injected with 5×10^3 GL261 cells, and mice brains were scanned by MRI at 17 and 21 days, as described in Materials and Methods. Images of representative WT (upper panel) and $Cd38^{-/-}$ (lower panel) mice taken at 21 days post-injection are shown in (A) and are displayed from frontal (left) to rostral (right). Tumor volume (B) was calculated, and a repeated-measures ANOVA revealed a significant effect for the genotype ($P = .001$). Tumor volume was significantly smaller in $Cd38^{-/-}$ mice at day 21 following injection compared with WT mice (*$P = .00001$, Fisher's least significant difference post-hoc test). Values are presented as the mean ± SEM (bars) ($n = 18$ WT and 16 $Cd38^{-/-}$ mice, respectively). The survival duration of the mice (C) was monitored. A Kaplan–Meier survival analysis of WT and $Cd38^{-/-}$ by a log-rank test revealed a significant difference between the survival durations of the 2 groups ($P = .0003$) ($n = 18$ WT and 16 $Cd38^{-/-}$ mice, respectively). For the aggressive glioma condition, mice were i.c. injected with 1×10^5 GL261 cells, and MRI was conducted at 10, 14, and 17 days post-injection. Images of representative WT (upper panel) and $Cd38^{-/-}$ (lower panel) mice taken at 17 days post-injection are shown in (D) and are displayed from frontal (left) to rostral (right). Tumor volume (E) was calculated at 10, 14, and 17 days post-injection. A repeated-measures ANOVA revealed a significant effect for the genotype ($P = .01$). Tumor volume was significantly smaller in $Cd38^{-/-}$ mice at day 17 following injection compared with WT mice (*$P = .00002$, Fisher's least significant

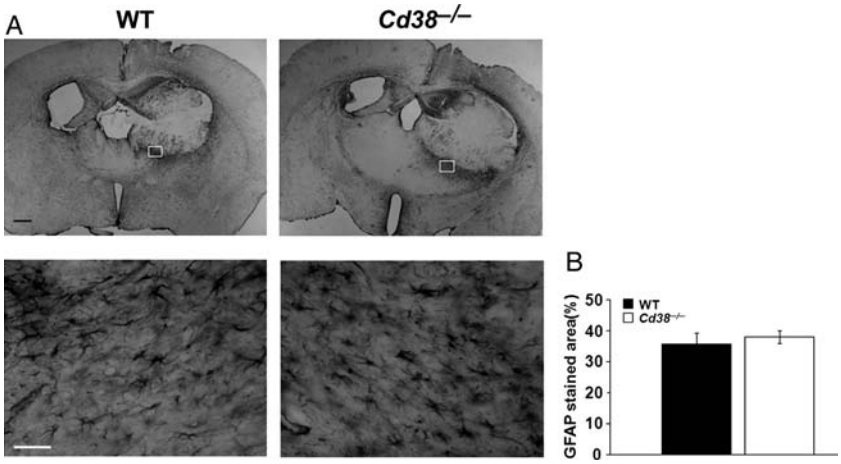

Fig. 2. Similar accumulation of astrocytes in the tumor boundaries in WT and $Cd38^{-/-}$ brains. WT and $Cd38^{-/-}$ mice were injected with 1×10^5 GL261 cells, and 20 days later sections were prepared and stained with anti-GFAP Abs. (A) Representative images of GFAP-stained tumor-containing brain sections of WT and $Cd38^{-/-}$ mice captured at 2× (upper panel) and 40× magnifications (lower panel). Rectangles indicate areas taken for 40× magnification. Scale bar = 500 μm or 50 μm for upper and lower panels, respectively. Quantitation of the density of the GFAP-positive cells in the tumor border (B) did not reveal a significant difference between the genotypes (Student's *t* test, $P = .29$). The results presented are from a representative experiment (of 2 independent sets of experiments). The values are presented as the mean ± SEM (bars) ($n = 7$).

obtained from the glioma-bearing hemisphere or control sham-injected hemisphere of WT mice. As shown in Fig. 4F, TMM express membrane CD38. Notably, the expression level of CD38 in the TMM was moderately (25%) but significantly higher than that of the control MM.

CD38 Deficiency Enhances Cell Death and Reduces MMP-12 Expression

Next, we investigated how CD38 deficiency in the tumor microenvironment can attenuate glioma progression. We first assessed cell proliferation and cell death in the tumor. To determine cell proliferation, we counted mitotic cells in the tumor area (Fig. 5A and B) or measured the density of BrdU staining in the tumor area (Fig. 5C and D). No significant difference was observed between WT and $Cd38^{-/-}$ glioma-bearing mice in either the number of mitotic cells or in the density of BrdU stained cells in the tumor area. These results suggest that the proliferation rate of the tumor cells in WT and $Cd38^{-/-}$ mice is similar and thus that the difference in the tumor size between the 2 genotypes does not seem to result from an effect of CD38 deficiency on cell proliferation. However, analysis of the amount of cell death in the tumor area by the TUNEL assay, which detects dead cells exhibiting fragmented DNA, revealed that the density of TUNEL-stained cells in the tumor area at day 20 was 50% higher in $Cd38^{-/-}$ than in WT mice (Fig. 5E and F). Since the survival of tumor cells depends inter alia on neovascularization in the tumor,[31] we examined whether the enhanced cell death observed in CD38 deficient mice is due to insufficient vascularization. To this end we assessed the amount of blood vessels in the tumor area by CD31 staining (a marker for endothelial cells). As shown in Fig. 5G and H, no significant difference was observed in the density of CD31 staining in the tumor area between WT and $Cd38^{-/-}$ glioma–bearing mice. These results thus suggest that vascularization in the tumor area is not affected by CD38 expression and thus that the enhanced cell death in the tumors of $Cd38^{-/-}$ glioma–bearing mice is mediated by other means.

Among the mechanisms that control glioma expansion is invasiveness, which is regulated inter alia by MMPs.[32] Because MMP-12 plays an important role in glioma invasion,[33] we examined whether MMP-12 expression in the tumor mass would be affected by CD38 deficiency. Brain sections obtained from glioma-bearing WT and $Cd38^{-/-}$ mice were stained with anti–MMP-12 Abs. As shown in Fig. 6A, in both *Cd38* genotypes there is a confined MMP-12 staining in the tumor mass that seems to be localized both intracellularly and extracellularly, as would be expected from a secreted

difference post-hoc test). Results shown are from a single experiment, and values are presented as the mean ± SEM (bars) ($n = 4$ WT and 8 $Cd38^{-/-}$ mice, respectively). (F) Comparison of the tumor volume at day 17 in WT and $Cd38^{-/-}$ mice. Values in each experiment were normalized to the average tumor volume in WT mice. The results are expressed as the mean ± SEM (bars) of the normalized tumor volumes of all the mice examined in 5 independent experiments ($n = 33$ WT and 30 $Cd38^{-/-}$ mice, respectively). The tumor volume was significantly smaller in $Cd38^{-/-}$ mice ($P = .002$, Student's *t* test). The survival duration of the mice (G) was monitored as described in Materials and Methods. A Kaplan–Meier survival analysis of WT and $Cd38^{-/-}$ by a log-rank test revealed a significant difference between the survival durations of the 2 groups ($P = .03$) ($n = 20$ and 17 for WT and $Cd38^{-/-}$ mice, respectively).

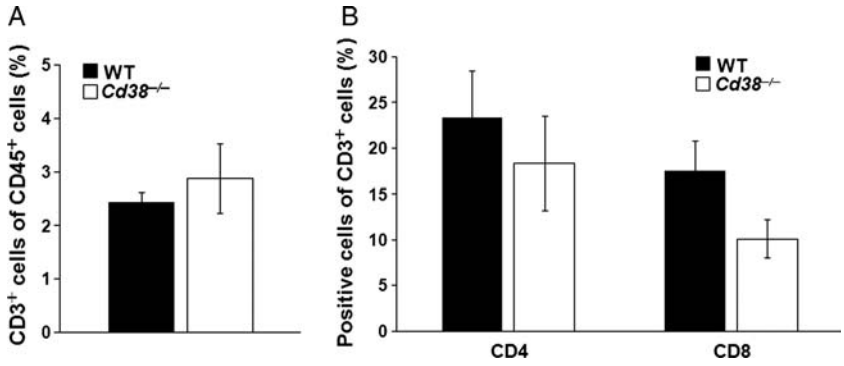

Fig. 3. Assessment of the T cells in WT and $Cd38^{-/-}$ mice. WT and $Cd38^{-/-}$ mice were injected with 1×10^5 GL261 cells; after 20 days, the brains were removed, processed, stained, and analyzed by flow cytometry. (A) The percentage of T cells ($CD3^+$) in the tumor-containing hemisphere was examined within the immune population (CD45 gated cells). Statistical analysis did not reveal a significant difference between the proportion of $CD3^+$ cells within the $CD45^+$ cell population in WT and $Cd38^{-/-}$ ($P = .27$, Student's t test). The data presented are expressed as the mean ± SEM; bars ($n = 8$ and 5 for glioma-injected WT and $Cd38^{-/-}$ mice, respectively). (B) The proportion of T-helper ($CD4^+$ cells) or cytotoxic T cells ($CD8^+$ cells) within the T cell population (CD3 gated cells) in the tumor-containing hemisphere. No significant difference was observed in the $CD4^+$ of the $CD3^+$ population between the genotypes ($P = .25$, Student's t test). The proportion of $CD8^+$ cells of the $CD3^+$ population was significantly higher in WT mice ($P = .04$, Student's t test). The data presented are expressed as the mean ± SEM; bars ($n = 8$ and 5 for glioma-injected WT and $Cd38^{-/-}$ mice, respectively).

protein such as MMP-12.[34] Assessment of the MMP-12 staining density in the tumor area revealed a modest (25%) but significant ($P = .05$) reduction in the staining density in the $Cd38^{-/-}$ mice compared with WT mice (Fig. 6B). These results suggest that CD38 deficiency leads to a reduction in MMP-12 levels in the tumor mass. To further substantiate this finding, MMP-12 levels were examined also by immunoblot analysis. Total protein extracts were prepared from tumor-bearing brain hemispheres and analyzed for MMP-12 expression. As shown in Fig. 6C, the 45-kDa active form of MMP-12 was detected in the WT and the $Cd38^{-/-}$ samples, whereas the proform of MMP-12 (55 kDa) was barely detected (not shown). Quantization of the amount of active MMP-12 in the different samples revealed that it was significantly ($P = .039$) lower (65%) in the $Cd38^{-/-}$ samples than in the WT samples. Taken together, these and the staining results suggest that CD38 deficiency reduces the amount of MMP-12 in the tumor mass. Among the cells that produce MMPs (including MMP-12) are MM[6]; therefore, we next examined whether CD38 deficiency may regulate glioma-induced expression of MMP-12 as well as other MMPs in TMM. We isolated MM or TMM (CD11b-positive cells) from sham- or tumor-injected brain hemispheres from WT or $Cd38^{-/-}$ mice, extracted their total RNA, and determined the mRNA levels of MMP-9, MMP-12, MMP-13, MMP-14, and MMP-19 by qRT-PCR. The analysis revealed that the tumor substantially induced the expression of MMP-14 and MMP-19 mRNAs in the TMM compared with MM isolated from sham-injected brains; however, no significant difference was observed in their mRNA levels in WT and $Cd38^{-/-}$ TMM (data not shown). MMP-12 and MMP-13 mRNA levels were also substantially higher in TMM compared with control MM; however, their mRNA levels were significantly lower (2-way ANOVA, $P = .01$ and $P = .014$, respectively) in $Cd38^{-/-}$ TMM compared with WT TMM (Fig. 7). Analysis of MMP-12 levels in protein extracts prepared from WT or $Cd38^{-/-}$ TMM (CD11b-positive cells) by immunoblotting revealed a trend toward a lower expression (28%) of active MMP-12 (45 kDa) in $Cd38^{-/-}$ TMM compared with WT TMM, but this effect was not significant ($P = .06$).

Discussion

The aim of the present study was to assess the role of CD38 in the tumor microenvironment on glioma progression. The results presented here show that CD38 deficiency delays glioma progression. Accordingly, CD38 deficiency substantially attenuated tumor growth and modestly but significantly prolonged the life span of glioma-bearing mice, suggesting that CD38 in the microenvironment plays a role in tumor progression.

The mechanism whereby CD38 deficiency affects glioma progression may involve, at least in part, alteration in the tumor-supporting activity of the TMM. This is supported by the observation that CD38 is expressed in TMM and that CD38 expression is higher in TMM than in MM. Furthermore, the results also show that CD38 deficiency does not affect the accumulation of TMM in the tumor but rather their features. The latter is suggested by the reduction not only in the density of F4/80 staining in the tumor area but also in the glioma-stimulated mRNA expression of MMP-12 and MMP-13. Importantly, it was shown previously that these MMPs regulate glioma invasion.[33,35] Notably, our findings also show that the amount of tumor-associated MMP-12 staining and expression of the 45-kDa active form was lower in glioma-bearing $Cd38^{-/-}$ mice compared with WT-glioma–bearing

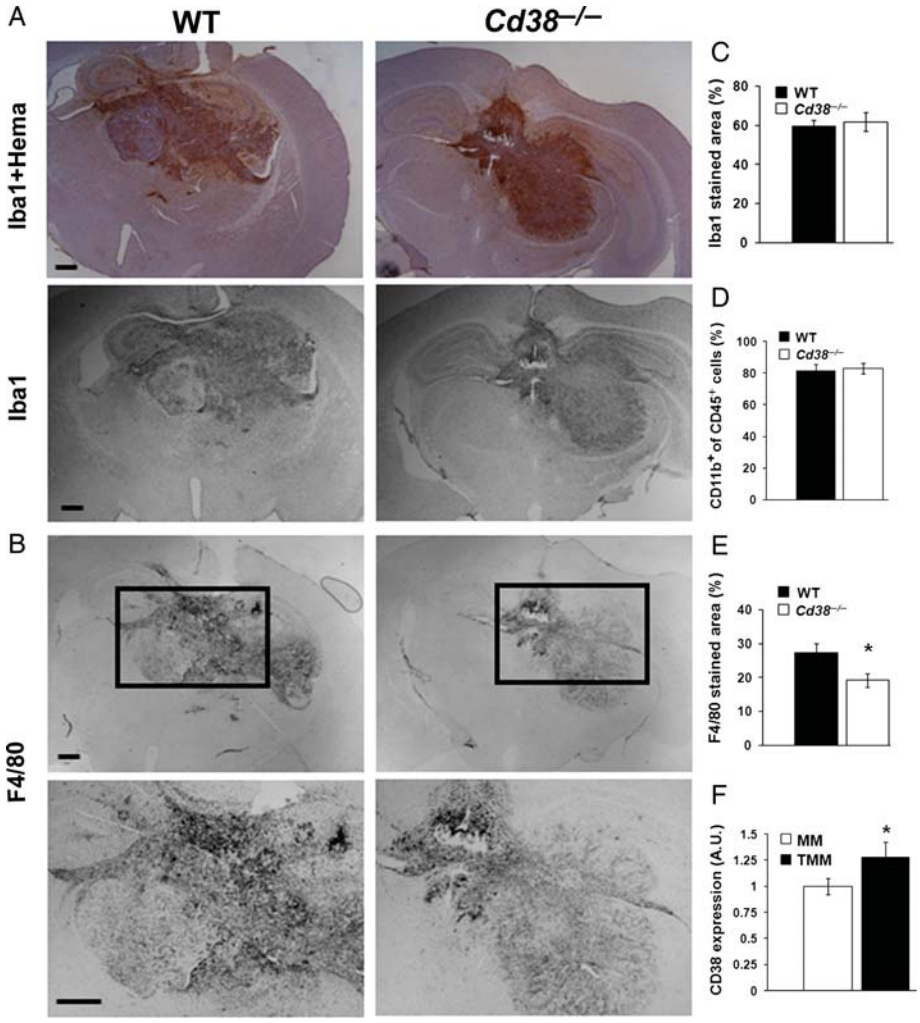

Fig. 4. MM in the tumor area in WT and $Cd38^{-/-}$ brains. Brain sections, prepared from WT and $Cd38^{-/-}$ mice i.c. injected with 1×10^5 GL261 cells 20 days earlier were immunostained with the anti-Iba1 (with or without counterstaining with hematoxylin) (A) or with anti-F4/80 Ab (B). The images in the lower panel of (B) are magnifications of the areas included in the rectangles in the upper panel. Scale bar = 500 μm. Quantitation of the density of the Iba1- or F4/80-positive cells in the tumor area is shown in (C) and (E), respectively. Statistical analysis revealed significant difference in the F4/80-stained area between the WT and $Cd38^{-/-}$ (Student's *t* test, $^*P = .01$) but not in the Iba1-stained area (Student's *t* test, $P = .36$). The data presented are expressed as the mean ± SEM; bars ($n = 9$ WT and 8 $Cd38^{-/-}$ mice, respectively). (D) Assessment of the MM cells in WT and $Cd38^{-/-}$ mice. WT and $Cd38^{-/-}$ glioma–bearing mice were processed for flow cytometry, as described in Fig. 3. The percentage of MM ($CD11b^+$) in the tumor-containing hemisphere was examined within the immune population (CD45 gated cells). No significant difference in the proportion of $CD11b^+$ cells within the $CD45^+$ cell population was observed between WT and $Cd38^{-/-}$ ($P = .38$, Student's *t* test). The data presented are expressed as the mean ± SEM; bars ($n = 8$ and 5 for glioma-injected WT and $Cd38^{-/-}$ mice, respectively). (F) Assessment of CD38 expression in MM and TMM. WT mice were injected with GL261 cells or DMEM (sham) and 20 days later brains were removed, processed, stained, and analyzed for CD38 expression by flow cytometry. Expression of CD38 in MM (CD11b gated cells isolated from sham-injected brains) and TMM (CD11b gated cells isolated from GL261-injected brains) was assessed as the mean fluorescence multiplied by the percent of cells expressing the protein. CD38 expression was higher in TMM than in MM ($^*P = .05$, Student's *t* test). The data presented are expressed as the mean ± SEM; bars $n = 4$ control samples (each pooled from 2 mice) and 8 glioma-injected mice.

mice. Although the MMP-12 measured in these experiments can originate from different cell types, it is feasible that at least part of it is derived from the TMM. Therefore, in view of the MMP-12 mRNA expression results, it is possible that the CD38-deficiency effect on MMP-12 levels in the tumor is mediated at least in part by the TMM. In this regard, it is important to note that analysis of MMP-12 protein levels in TMM ($CD11b^+$-positive cells) revealed only a trend ($P < .06$) toward reduction in the level of MMP-12 protein in $Cd38^{-/-}$ TMM compared with WT TMM. Since the results did not reach statistical significance, it is uncertain whether $Cd38^{-/-}$ TMM indeed synthesize lower amounts of MMP-12 protein compared with

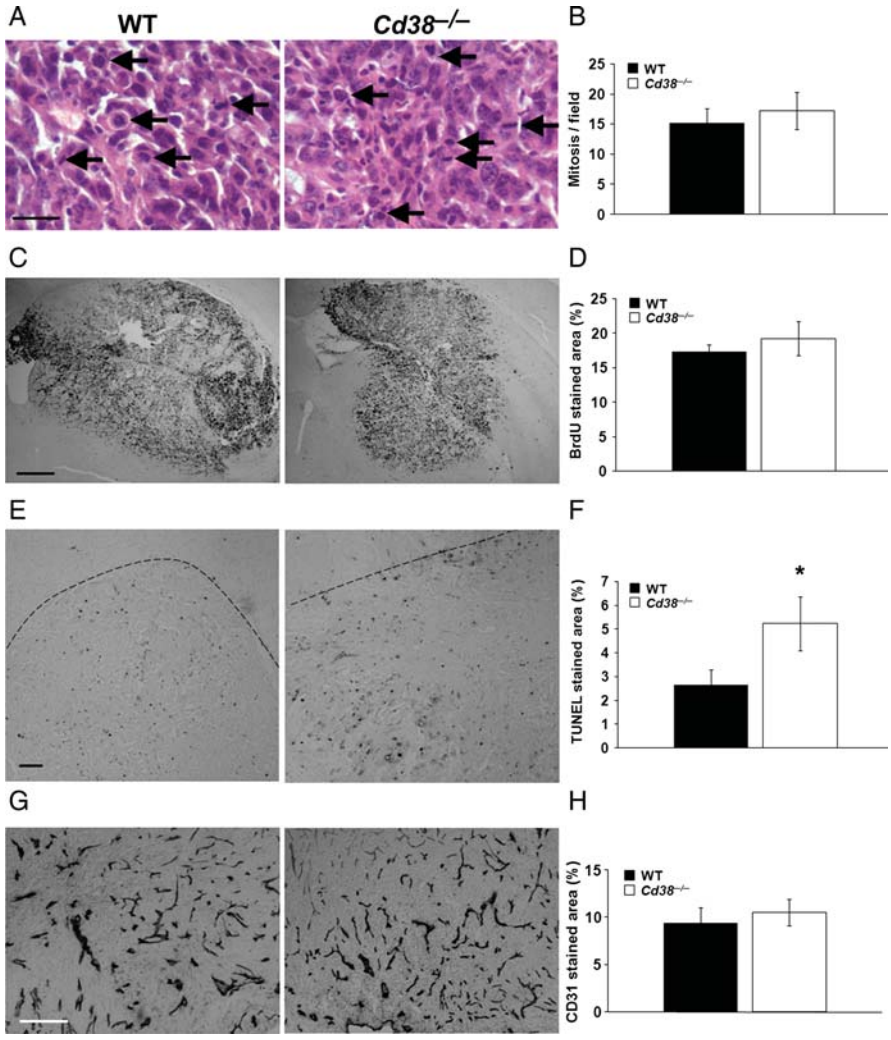

Fig. 5. The effect of CD38 deficiency on tumor features. WT and $Cd38^{-/-}$ mice were i.c. injected with 1×10^5 GL261 cells. Brain sections were counterstained with H&E (A), immunohistochemically stained with anti-BrdU (C), anti-CD31 (G) Abs or TUNEL reagent (E) as described in Materials and Methods. Proliferation was assessed using (A) mitotic cell counting in H&E stained sections (scale bar = 25 μm); (representative mitotic cells are indicated by arrows) and (C) by BrdU staining (scale bar = 500 μm). Quantitation of the number of mitotic cells (B) or BrdU staining of the tumor area (D) did not reveal a significant difference between the genotypes (Student's *t* test, $P = .31$ and $P = .27$, respectively). The data presented are expressed as the mean ± SEM (bars), ($n = 4$ for H&E and $n = 9$ WT and 8 $Cd38^{-/-}$ mice for BrdU staining). Cell death was assessed by the TUNEL assay (E), (scale bar = 100 μm). Quantitation of the density of the TUNEL positive cells in the tumor area (F) revealed that the percentage of the tumor area stained by TUNEL was significantly higher in $Cd38^{-/-}$ mice (*$P = .05$, Student's *t* test). Results shown are from a representative experiment of 2 independent sets of experiments that yielded similar results. The values are presented as the mean ± SEM (bars) ($n = 4$). The dotted line represents the tumor border. Vascularization was assessed by the anti-CD31 Ab (G), scale bar = 250 μm. Quantitation of the density of the CD31 positive cells in the tumor area (H) did not reveal a significant difference between the genotypes (Student's *t* test, $P = .48$). The data presented are expressed as the mean ± SEM (bars), ($n = 7$ WT and 6 $Cd38^{-/-}$ mice).

WT TMM, as would be expected from the mRNA analysis. However, owing to the TMM isolation procedure, we most likely measure only a subpopulation of this secreted protein, ie, the cellular MMP-12. In addition to MMP-12 and MMP-13, other MMPs such as MT1-MMP (MMP-14)[6] were shown to play an important role in the effect of TMM on glioma expansion. Our results, however, did not reveal an effect of CD38 on the glioma-induced mRNA expression of MMP-14. The notion that at least some of the CD38 deficiency effects on glioma progression are mediated via modulation of the glioma-supporting role of the TMM is further supported by the lack of CD38-dependent changes in the amount of astrocytes and T cells in the tumor area. However, we cannot exclude the possibility that other cells play a role in the CD38-deficiency effect on glioma progression or that CD38 deficiency affects the functionality, but not the amount, of microenvironment cells. Further studies are needed to assess this possibility.

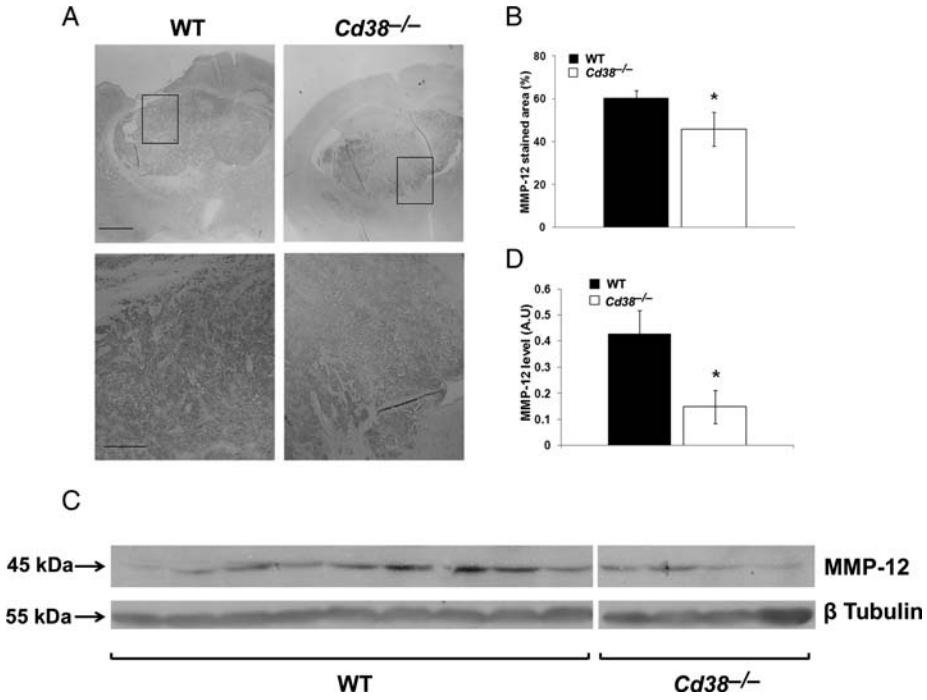

Fig. 6. Reduced MMP-12 levels in tumors of $Cd38^{-/-}$ mice. WT and $Cd38^{-/-}$ mice were i.c. injected with 1×10^5 GL261 cells. (A) Brain sections were stained with anti-MMP-12 Abs as described in Materials and Methods. The images in the lower panel are magnifications of the areas included in the rectangles in the upper panel (scale bar = 500 and 250 μm, respectively). (B) Quantitation of the density of MMP-12 staining revealed a significant difference between WT and $Cd38^{-/-}$ mice (*$P = .05$, Student's t test) ($n = 6$ WT and 5 $Cd38^{-/-}$ mice). (C) WT and $Cd38^{-/-}$ mice were i.c. injected with 5×10^3 GL261 cells. At day 29, brains were removed, proteins were extracted from the tumor-bearing hemisphere, and MMP-12 levels were examined by immunoblotting as described in the Materials and Methods. (D) MMP-12 levels are expressed as signal-intensity values (normalized to β-Tubulin). Expression levels were significantly lower in $Cd38^{-/-}$ mice compared with WT (*$P = .039$, Student's t test) ($n = 9$ WT and 4 $Cd38^{-/-}$ mice).

Our finding that CD38 deficiency enhances cell death and reduces MMP expression (at least MMP-12) in the tumor mass suggests that the effect of CD38 deficiency on the tumor is multifunctional and may involve various pathways such as cell death and invasiveness. How CD38 deficiency in the tumor microenvironment enhances cell death is not known. A possible mechanism could be via lack of sufficient vascularization. This, however, does not seem to be the case because we did not observe differences in the densities of CD31 staining in the tumor area between WT and $Cd38^{-/-}$ mice. In addition, we did not observe CD38-dependent differences in expression of apoptotic proteins (eg, active caspase-3, Bax, Bak, and Bcl-x_L) (data not shown) in protein extracts prepared from the tumor-bearing hemisphere. Thus CD38 deficiency in the glioma microenvironment does not alter the expression of at least these important components of the apoptotic machinery. Other tumor microenvironment-associated agents that may contribute to the enhanced cell death effect may be lack of survival factors and/or cytotoxic molecules such as NO. Further studies are needed to assess these possibilities.

CD38 is one of the major NADases in mammalian tissues; thus CD38 deficiency may lead to enhancement in NAD levels in tissues[36] of $Cd38^{-/-}$ mice and the tumor microenvironment. It was shown previously that NAD can exert toxic effects in some systems.[37,38] Thus CD38 deficiency might regulate glioma progression by promoting NAD-induced glioma cell death. Although we cannot exclude this possibility, we do not favor it because treatment of GL261 cells in vitro with 1 or 10 μM NAD for 48 h did not affect the viability of the cells (data not shown).

We show here that CD38 deficiency in the glioma microenvironment attenuates glioma expansion. This result also supports the notion that the glioma microenvironment, probably by the action of (but not necessarily exclusively) TMM, supports glioma progression.[39] In view of the ineffectiveness of the current anti-glioma treatments, which are aimed largely against the tumor cells, an alternative approach based on targeting the supporting microenvironment might have a therapeutic benefit. Our results suggest that CD38 might be such a target. Although the effect of CD38 depletion by itself is not curative, it is feasible that a combination of targeting CD38 (in the tumor microenvironment) and the glioma tumor cells will have a synergistic impact on glioma progression and be used in the future as a potential therapeutic approach for glioma therapy.

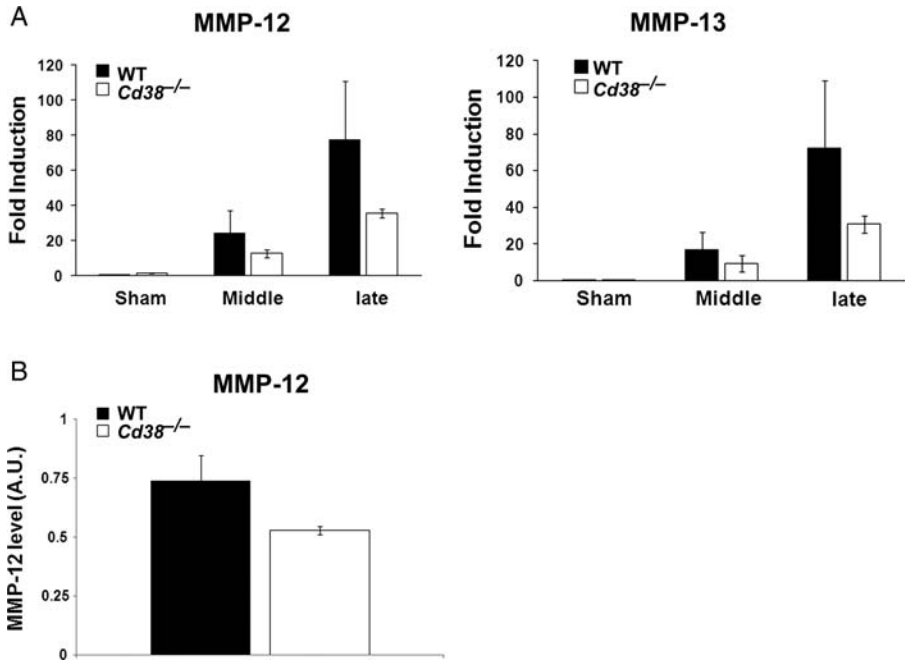

Fig. 7. The effect of CD38 deficiency on MMP-12 and MMP-13 expression in TMM. (A) CD38 deficiency attenuates the glioma-induced expression of MMP-12 and MMP-13 mRNA levels. WT and $Cd38^{-/-}$ mice were i.c. injected with DMEM (sham) or 1×10^5 GL261 cells, and 18, 20, or 22 days later brains were removed for isolation of MM (from sham-injected brains) or TMM (from glioma-injected brains). RNA extraction from the isolated cells was performed as described in Materials and Methods. Data collected from the different TMM samples were classified into 2 groups, one corresponding to TMM isolated from middle phase/size tumor (Middle) and the second large phase/size tumor (Large) as described in Materials and Methods. Comparison of MMP-12 and MMP-13 mRNA levels by the $2^{-\Delta\Delta CT}$ method revealed a significant effect for the genotype (2-way ANOVA, $P = .01$ and $P = .014$, respectively). The values are presented as the mean fold induction $\pm$ SEM (bars) relative to WT sham: $n = 3$ (each TMM sample is a pool from 3 brains, whereas the MM samples each pool 4–5 brains). (B) Examination of MMP-12 protein expression. WT and $Cd38^{-/-}$ mice were i.c. injected as described above. TMM were isolated on day 20, proteins were extracted, and MMP-12 expression was examined by immunoblotting as described in Materials and Methods. MMP-12 expression levels (45 kDa active form) are expressed as signal-intensity values (normalized to GAPDH). Statistical analysis revealed a trend toward reduced MMP-12 levels in $Cd38^{-/-}$ TMM (Student's t test, $P = .06$). The values are presented as the mean $\pm$ SEM (bars): $n = 3$ (each TMM sample is a pool from 2–4 brains).

Supplementary Material

Supplementary material is available at *Neuro-Oncology Journal* online (http://neuro-oncology.oxfordjournals.org/).

Acknowledgments

We thank the Alfredo Federico Strauss Center For Computational Neuro-Imaging at Tel Aviv University.

Conflict of interest statement. None declared.

Funding

The MRI scanner used in this study was purchased with grants from the Israel Science Foundation and from the Raymond and Beverly Sackler Institute of Biophysics of Tel Aviv University. This work is supported in part by The U.S.-Israel Binational Science Foundation (2007061 to R.S. and F.L.); the Israel Ministry of Science, Culture, and Sport (Eshkol Foundation to L.M.); the Chief Scientist Office of the Ministry of Health, Israel (grant no. 3-7290) (to R.S.); the Adams Super-Center for Brain Research (to R.S.); the Tel Aviv University Cancer Biology Research Center (to A.L.); and the National Institutes of Health (R01 AI063399 to F.L.).

References

1. Badie B, Schartner J. Role of microglia in glioma biology. *Microsc Res Tech*. 2001;54:106–113.
2. Rivest S. Regulation of innate immune responses in the brain. *Nat Rev Immunol*. 2009;9:429–439.
3. Watters JJ, Schartner JM, Badie B. Microglia function in brain tumors. *J Neurosci Res*. 2005;81:447–455.
4. Yang I, Han SJ, Kaur G, Crane C, Parsa AT. The role of microglia in central nervous system immunity and glioma immunology. *J Clin Neurosci*. 2010;17:6–10.
5. Markovic DS, Glass R, Synowitz M, Rooijen N, Kettenmann H. Microglia stimulate the invasiveness of glioma cells by increasing the activity of metalloprotease-2. *J Neuropathol Exp Neurol*. 2005;64:754–762.

6. Markovic DS, Vinnakota K, Chirasani S, et al. Gliomas induce and exploit microglial MT1-MMP expression for tumor expansion. *Proc Natl Acad Sci USA*. 2009;106:12530–12535.
7. Mayo L, Jacob-Hirsch J, Amariglio N, et al. Dual role of CD38 in microglial activation and activation-induced cell death. *J Immunol*. 2008; 181:92–103.
8. Partida-Sanchez S, Iribarren P, Moreno-Garcia ME, et al. Chemotaxis and calcium responses of phagocytes to formyl peptide receptor ligands is differentially regulated by cyclic ADP ribose. *J Immunol*. 2004;172:1896–1906.
9. Franco L, Bodrato N, Moreschi I, et al. Cyclic ADP-ribose is a second messenger in the lipopolysaccharide-stimulated activation of murine N9 microglial cell line. *J Neurochem*. 2006;99:165–176.
10. Levy A, Bercovich-Kinori A, Alexandrovich AG, et al. CD38 facilitates recovery from traumatic brain injury. *J Neurotrauma*. 2009;26: 1521–1533.
11. Malavasi F, Deaglio S, Funaro A, et al. Evolution and function of the ADP ribosyl cyclase/CD38 gene family in physiology and pathology. *Physiol Rev*. 2008;88:841–886.
12. Partida-Sanchez S, Rivero-Nava L, Shi G, Lund FE. CD38: an ecto-enzyme at the crossroads of innate and adaptive immune responses. *Adv Exp Med Biol*. 2007;590:171–183.
13. Partida-Sanchez S, Cockayne DA, Monard S, et al. Cyclic ADP-ribose production by CD38 regulates intracellular calcium release, extracellular calcium influx and chemotaxis in neutrophils and is required for bacterial clearance in vivo. *Nat Med*. 2001;7:1209–1216.
14. Guedes AG, Paulin J, Rivero-Nava L, Kita H, Lund FE, Kannan MS. CD38-deficient mice have reduced airway hyperresponsiveness following IL-13 challenge. *Am J Physiol Lung Cell Mol Physiol*. 2006;291:L1286–L1293.
15. Kato I, Yamamoto Y, Fujimura M, Noguchi N, Takasawa S, Okamoto H. CD38 disruption impairs glucose-induced increases in cyclic ADP-ribose, [Ca2 +]i, and insulin secretion. *J Biol Chem*. 1999;274:1869–1872.
16. Sun L, Iqbal J, Dolgilevich S, et al. Disordered osteoclast formation and function in a CD38 (ADP-ribosyl cyclase)-deficient mouse establishes an essential role for CD38 in bone resorption. *FASEB J*. 2003;17:369–375.
17. Jin D, Liu HX, Hirai H, et al. CD38 is critical for social behaviour by regulating oxytocin secretion. *Nature*. 2007;446:41–45.
18. Partida-Sanchez S, Randall TD, Lund FE. Innate immunity is regulated by CD38, an ecto-enzyme with ADP-ribosyl cyclase activity. *Microbes Infect*. 2003;5:49–58.
19. Malavasi F, Deaglio S, Damle R, Cutrona G, Ferrarini M, Chiorazzi N. CD38 and chronic lymphocytic leukemia: a decade later. *Blood*. 2011;118:3470–3478.
20. Cockayne DA, Muchamuel T, Grimaldi JC, et al. Mice deficient for the ecto-nicotinamide adenine dinucleotide glycohydrolase CD38 exhibit altered humoral immune responses. *Blood*. 1998;92:1324–1333.
21. Krebs C, Adriouch S, Braasch F, et al. CD38 controls ADP-ribosyltransferase-2-catalyzed ADP-ribosylation of T cell surface proteins. *J Immunol*. 2005;174:3298–3305.
22. Miyoshi H, Takahashi M, Gage FH, Verma IM. Stable and efficient gene transfer into the retina using an HIV-based lentiviral vector. *Proc Natl Acad Sci USA*. 1997;94:10319–10323.
23. Matsumori Y, Hong SM, Fan Y, et al. Enriched environment and spatial learning enhance hippocampal neurogenesis and salvages ischemic penumbra after focal cerebral ischemia. *Neurobiol Dis*. 2006;22:187–198.
24. Cardona AE, Huang D, Sasse ME, Ransohoff RM. Isolation of murine microglial cells for RNA analysis or flow cytometry. *Nat Protoc*. 2006;1:1947–1951.
25. Hickman SE, Allison EK, El Khoury J. Microglial dysfunction and defective beta-amyloid clearance pathways in aging Alzheimer's disease mice. *J Neurosci*. 2008;28:8354–8360.
26. Livak KJ, Schmittgen TD. Analysis of relative gene expression data using real-time quantitative PCR and the 2(-Delta Delta C(T)) m vb nbethod. *Methods*. 2001;25:402–408.
27. Lukasiak S, Breuhahn K, Schiller C, Schmidtke G, Groettrup M. Quantitative analysis of gene expression relative to 18S rRNA in carcinoma samples using the LightCycler instrument and a SYBR GreenI-based assay: determining FAT10 mRNA levels in hepatocellular carcinoma. *Methods Mol Biol*. 2008;429:59–72.
28. Dixon WJ, Massey FJ. Introduction to Statistical Analysis. 1st ed. New York: McGraw-Hill; 1951.
29. Newcomb EW, Zagzag D. The murine GL261 glioma experimental model to assess novel brain tumor treatments. In: Meir, EG, ed. *CNS Cancer: Models, Markers, Prognostic Factors, Targets and Therapeutic Approaches*. Dordrecht: Springer; 2009:227–241.
30. Szatmari T, Lumniczky K, Desaknai S, et al. Detailed characterization of the mouse glioma 261 tumor model for experimental glioblastoma therapy. *Cancer Sci*. 2006;97:546–553.
31. Folkman J. Tumor angiogenesis: therapeutic implications. *N Engl J Med*. 1971;285:1182–1186.
32. Nakada M, Okada Y, Yamashita J. The role of matrix metalloproteinases in glioma invasion. *Front Biosci*. 2003;8:e261–e269.
33. Sarkar S, Nuttall RK, Liu S, Edwards DR, Yong VW. Tenascin-C stimulates glioma cell invasion through matrix metalloproteinase-12. *Cancer Res*. 2006;66:11771–11780.
34. Belaaouaj A, Shipley JM, Kobayashi DK, et al. Human macrophage metalloelastase. Genomic organization, chromosomal location, gene linkage, and tissue-specific expression. *J Biol Chem*. 1995;270: 14568–14575.
35. Yeh WL, Lu DY, Lee MJ, Fu WM. Leptin induces migration and invasion of glioma cells through MMP-13 production. *Glia*. 2009;57: 454–464.
36. Chini EN. CD38 as a regulator of cellular NAD: a novel potential pharmacological target for metabolic conditions. *Curr Pharm Des*. 2009;15:57–63.
37. Adriouch S, Hubert S, Pechberty S, Koch-Nolte F, Haag F, Seman M. NAD + released during inflammation participates in T cell homeostasis by inducing ART2-mediated death of naive T cells in vivo. *J Immunol*. 2007;179:186–194.
38. Ying W. NAD + /NADH and NADP + /NADPH in cellular functions and cell death: regulation and biological consequences. *Antioxid Redox Signal*. 2008;10:179–206.
39. Barcellos-Hoff MH, Newcomb EW, Zagzag D, Narayana A. Therapeutic targets in malignant glioblastoma microenvironment. *Semin Radiat Oncol*. 2009;19:163–170.